TRANSIENT 3D SIMULATION OF HEAT TRANSFER FROM SPHERICAL AND STRONGLY DEFORMED DROPLETS AT HIGH REYNOLDS NUMBERS

M. Hase and B. Weigand
Institute of Aerospace Thermodynamics, University of Stuttgart,
Pfaffenwaldring 31, 70569 Stuttgart, Germany

Abstract
A numerical study of heat transfer on droplets with an initial deformation at high Reynolds number is described. The two-phase flow is computed with a 3D DNS program using the Volume-of-Fluid method. For the droplets initial prolate and oblate shapes with an axial approaching flow are investigated. Additionally a spherical shape is used as reference. The initial droplet Reynolds number for the present study is $Re_0 = 660$ for all investigated cases. Due to the fact that the steady droplet velocity for the considered droplets is much lower than the initial velocity of the droplets, the droplet velocity is decreasing during the simulation. To gain more knowledge about the influence of deformation on the heat transfer, the time dependent, spatial averaged Nusselt number Nu_t and the time and spatial averaged Nusselt number Nu_m is matched with the temperature and velocity field around a deformed droplet. By this comparison the oscillation phase with the largest heat transfer is observed. As another important parameter the droplet surface is taken into account.

Introduction

The rate of heat transfer from the surrounding gas to droplets in sprays is a critical design parameter of many technical spray systems as for instance in automotive engines or gas turbines. In these processes the considered droplets respectively liquid ligaments are in many cases strongly deformed and the droplet velocity is heavily unsteady. Additionally due to the high velocities the flow around the droplet is transient and fully 3D. Because of this difficulties strongly deformed droplets have been studied rarely in the past, neither numerically nor experimentally.

In the present study it has been assumed that the droplets are deformed initially due to the primary breakup. During this breakup process strongly deformed liquid ligaments emerge which are approximated by two idealized droplet shapes in this study as a first step. The numerical investigation has been performed at high Reynolds numbers ($Re > 270$), which means that the flow is fully 3D and time dependent. The initial Reynolds number $Re_0 = D_0 U_0 / \nu_d$ of the considered droplets is $Re_0 = 660$, where D_0 is the diameter of a spherical droplet with the same volume, U_0 the initial droplet velocity and ν_d the kinematic viscosity of the disperse phase. To take the 3D flow character into account the investigation has been performed fully 3D. Additionally no restrictions on the deformation of the droplets is assumed. The programs efficiency and reliability for the computation of strongly deformed two-phase flow has been presented already in [1].

Analysis and numerical method

The inhouse 3D CFD program FS3D (Free Surface 3D) has been developed to compute the Navier-Stokes equations for incompressible flows with free surfaces. The equations are solved without using a turbulence model by *Direct Numerical Simulation* (DNS). The governing conservation equations for momentum and mass are

$$\frac{\partial(\rho \mathbf{u})}{\partial t} + \nabla \cdot [(\rho \mathbf{u}) \otimes \mathbf{u}] = -\nabla p + \nabla \cdot \mu \left[\nabla \mathbf{u} + (\nabla \mathbf{u})^T\right] + \nabla \cdot \mathbf{T} \quad (1)$$

$$\nabla \cdot \mathbf{u} = 0 \quad , \quad (2)$$

where $\mathbf{T}$ is the capillary stress tensor which adds the surface tensor force to the momentum equation. Furthermore $\mathbf{u}$, ρ, μ and p are the velocity vector, the density, the dynamic viscosity and the pressure, respectively.

Additionally the energy equation is solved. For the above mentioned incompressible flow and for a fluid with constant fluid properties in each phase the energy equation is decoupled from the equations of motion. Therefore, the energy equation can be solved after the computation of the flow field. The energy equation has been implemented in the temperature form

$$\frac{\partial}{\partial t}(\rho c_p T) + \nabla \cdot (\rho c_p \mathbf{u} T) = \nabla \cdot (\lambda \nabla T) + \Phi \quad . \quad (3)$$

where T is the temperature, c_p the specific heat and λ the heat conductivity. The dissipation term Φ can be neglected for all mentioned flows due to the low Eckert number. The implementation and validation of the energy equation has been described in [2].

In two phase flows additional information about the interface position between the disperse and the continuous phase are needed. There are two different approaches to manage this task. The first one is the explicit tracking of the interface (Front-Tracking) and the other is the tracking of the disperse phase (Volume-Tracking). In FS3D a Volume-Tracking method, well known as the *Volume-of-Fluid* (VOF) method, is used [3]. In the VOF-method an additional transport equation

$$\frac{\partial f}{\partial t} + \nabla \cdot (\mathbf{u} f) = 0 \tag{4}$$

for the volume fraction of the disperse phase is solved. The variable f is called the VOF-variable. The VOF-variable is

$$f = \begin{cases} 0 & \text{in the continuous phase} \\ 0 < f < 1 & \text{at the interface} \\ 1 & \text{in the disperse phase} \end{cases} \tag{5}$$

With the VOF-variable the change of the fluid properties across the interface can be computed by using the equations

$$\rho(\mathbf{x},t) = \rho_d + (\rho_c - \rho_d)\, f(\mathbf{x},t) \tag{6}$$

$$\mu(\mathbf{x},t) = \mu_d + (\mu_c - \mu_d)\, f(\mathbf{x},t) \tag{7}$$

where the subscript c indicates the continuous phase and d the disperse phase. Additional fluid properties like the specific heat c_p and the heat conductivity λ are obtained in the same way with the VOF-variable. To ensure a sharp interface and to suppress numerical dissipation of the disperse phase in each time step the interface is reconstructed with the PLIC-method (*Piecewise linear interface reconstruction computation*) [4]. After the reconstruction, the disperse phase is transported on the basis of the reconstructed distribution of the disperse phase.

The spatial discretization is realized by a structured Finite Volume scheme on a staggered grid. In each phase the discretization is second-order accurate. Due to the high gradients across the interface a limiter is used to prevent the generation of oscillations and spurious solutions. The program is parallelized with domain decomposition using the communication library *MPI*. A multigrid solver is included to solve the Poisson equation for the pressure. Additionally a coordinate transformation from the inertial system to the droplet system is implemented [5] to track the droplet for a longer time without generating very large computational domains.

Results

In the presented simulations, the liquid has been assumed to have the properties of water at $20°C$ except for the dynamic viscosity. The dynamic viscosity is $\mu_L = 10 \cdot \mu_{H_2 0} = 1 \cdot 10^{-3}\,\mathrm{kg/(ms)}$. The higher viscosity has been chosen to avoid *parasitic currents* [6]. For the surrounding gas the properties of air have been chosen. The initial temperature of the liquid was $T_L = 350\,K$ and $T_G = 293.15\,K$ for the gaseous phase.

The computational domain is displayed in Fig. 1. The 3D channel geometry for a spherical droplet with the diameter $D = 1 \cdot 10^{-3}\,m$ is $x = 12 \cdot 10^{-3}\,m$, $y = 6 \cdot 10^{-3}\,m$ and $z = 6 \cdot 10^{-3}\,m$. The gravitational force acts in the negative x-direction.

To perform the study concerning the heat transfer of deformed droplets, two initially strongly deformed droplets have been computed. One is a cylinder with diameter $D = 0.451 \cdot 10^{-3}\,m$ and the cylinders axis parallel to the flow direction. The other initial shape is a disk with diameter $D = 1.38 \cdot 10^{-3}\,m$ with the flow direction perpendicular to the disk surface. The volume of this droplets are the same as for a droplet with $D = 1 \cdot 10^{-3}\,m$.

In Fig. 2 the surface area of the three different initial droplet shapes in dependency of the Fourier number $Fo = at/R_0^2$ is displayed, where a, t, R_0 are the thermal diffusivity, the time and the radius of the spherical droplet with the same volume, respectively. For both deformed droplets oscillations can be seen, which were damped over the time. At $Fo = 0.01$ nearly the same surface area as a spherical droplet has been reached for the deformed droplets. The marks in Fig. 2 indicate the Fourier numbers used in Figs. 3 and 4.

In Fig. 3 the temporal evolution of the droplet shape and the temperature field for the initial cylindrical droplet is shown at different times. Additionally the velocity field around the droplet is displayed. The droplet shape and the temperature field for an initial disk shaped droplet is displayed in Fig. 4. The figures give an impression of the evolution of the temperature field due to the deformation of the droplet and due to the flow field. At $Fo = 0$ the initial conditions for both shapes can be seen. The disk shaped droplet passed through a half oscillation period at the next displayed time $Fo = 0.00108$ to a prolate shape as depicted in Fig. 4b. The initial cylindrical droplet in 3b is still cylindrical at this time. At $Fo = 0.00108$ a very interesting difference in

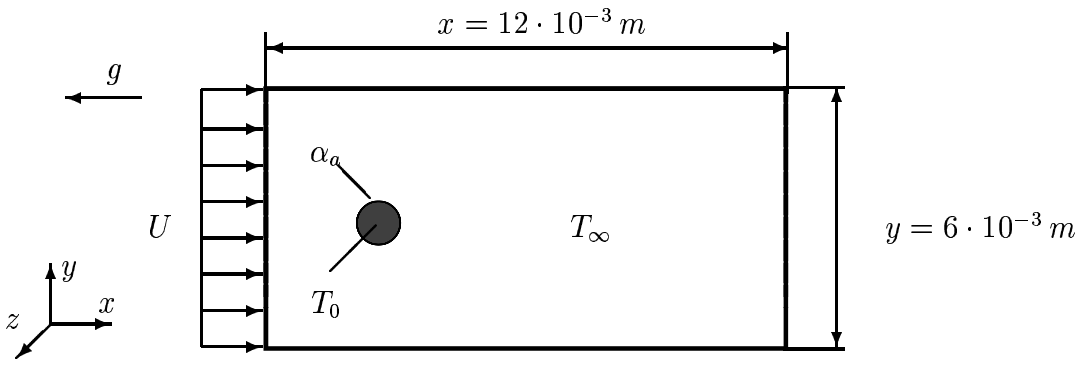

FIGURE 1: Channel geometry and boundary conditions for a computation of a droplet diameter of $D = 1 \cdot 10^{-3}\, m$.

the temperature field can be seen. In Fig. 3b a significant increase in the gas temperature occurs behind the droplet. But for the initial disk shape droplet (Fig. 4b) the temperature increase is weak. At $Fo = 0.00202$ in Fig. 3c the initial cylindrical droplet is oscillating from an oblate to a prolate shape short-time after the largest oblate deformation (see Fig. 2). The temperature distribution behind this droplet is similar to the initial disk shape in Fig. 4c at the same time, but the temperature is higher for the cylindrical case. The droplet in Fig. 4c at $Fo = 0.00202$ is oscillating from prolate to oblate shape (see Fig. 2). The displayed droplet will immediately reach the largest oblate deformation. As pointed out later, the highest heat transfer occurs during the oscillation to the oblate shape. Due to the time delay by the heat transport in the gas phase the effect of the higher heat transfer on the gas temperature is more significant after the droplet passed through the largest oblate deformation. In Fig. 3c it can also be seen, that directly behind the droplet the temperature is lower than in the vortices in the recirculation zone. This clarifies that after a period of high heat transfer a period of lower heat transfer is following. Fig. 3d and Fig. 4d at $Fo = 0.00337$ shows nicely the fully 3D character of the flow and temperature field.

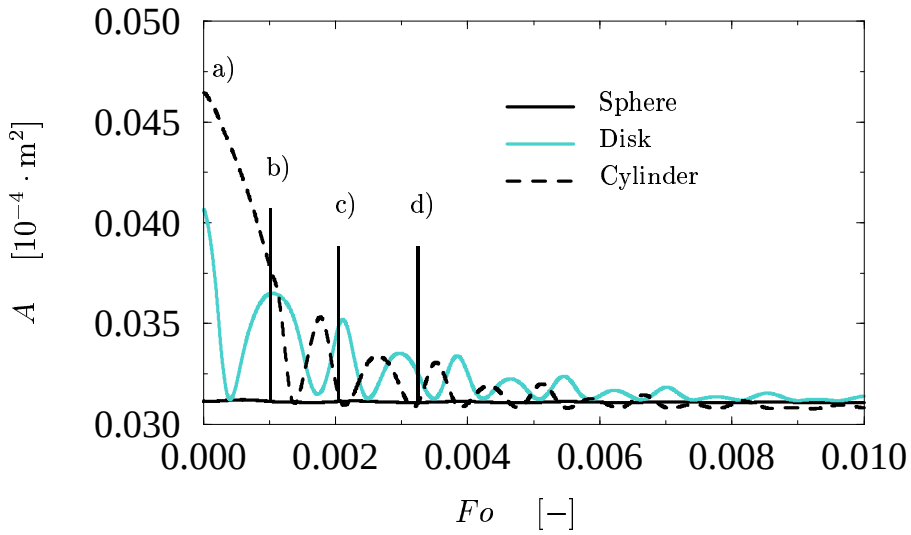

FIGURE 2: Surface area A for three different, initial deformed droplets with $\mu_L = 10 \cdot \mu_{H_2 0}$ as a function of Fo.

As mentioned before, in Fig. 2 the surface area in dependency of Fo is displayed for three different initial droplet shapes. The initial droplet area of the cylindrical droplet is larger than the surface area of the discoidal droplet. Nevertheless no difference in the mean Nusselt number evolution in Fig. 5, where the time and spatial averaged Nusselt number is shown in dependency of Fo, can be seen. In the computation of the Nusselt number Nu_m the real surface area has been taken into account by computing the heat flux density according to

$$\dot{q} = \frac{\rho_L c_{p,L} V}{A} \frac{T_1 - T_0}{t_1 - t_0} \quad , \tag{8}$$

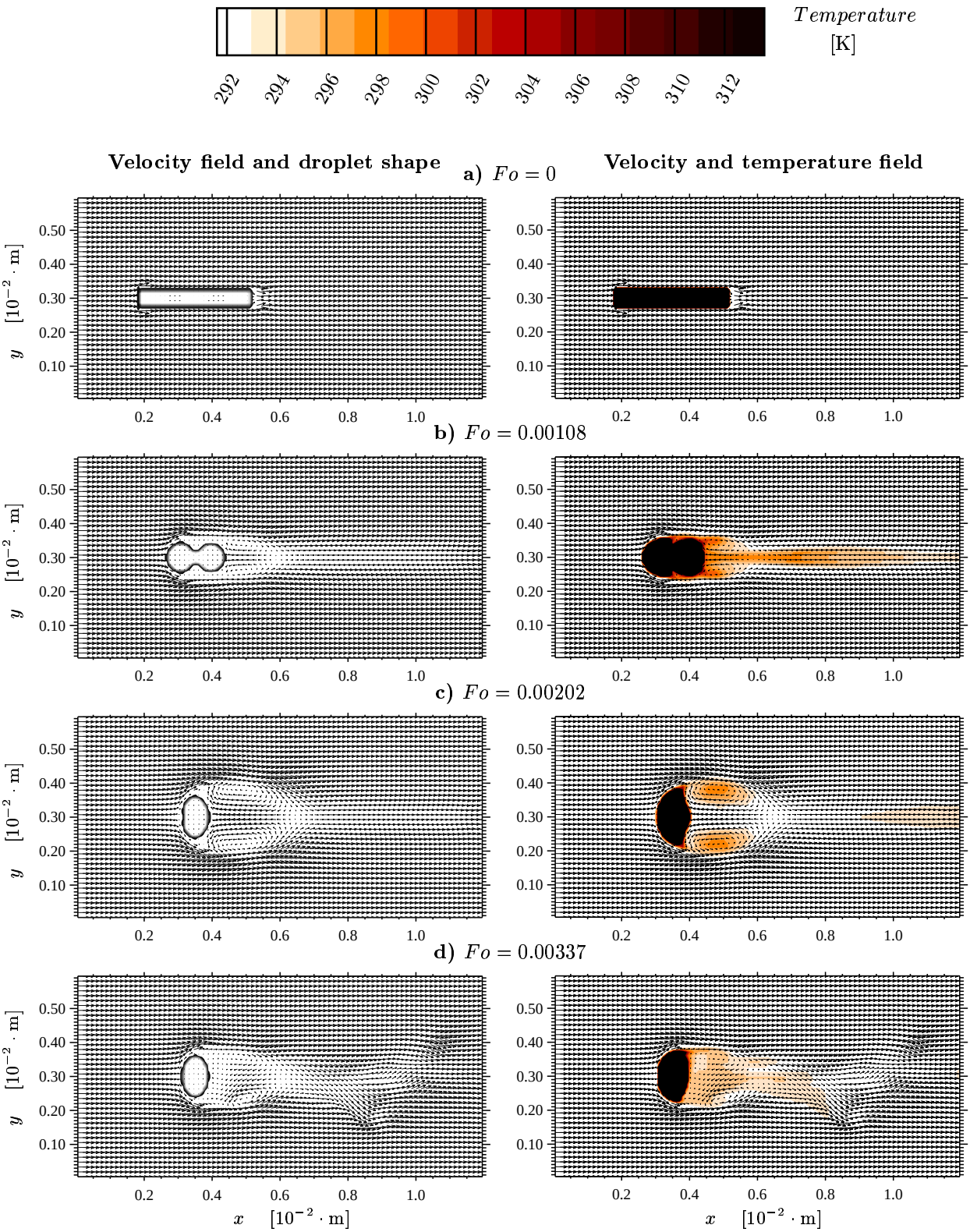

FIGURE 3: Velocity field and temperature field around a initial cylindrical droplet with the diameter $D = 1 \cdot 10^{-3}$ in dependency of Fo.

where A is the real surface area of the deformed droplet, V the droplet volume and the subscripts 0,1 are the initial and the current state of time t and temperature T. Therefore, the results from Fig. 2 and Fig. 5 confirm the heat transfer performance for the discoidal and the cylindrical droplet as seen from Fig. 3b and Fig. 4b. The heat flux $\dot{Q}$ which does not contain the larger surface area of the cylindrical droplet, is higher for the cylindrical case.

In addition averaged Nusselt numbers Nu_m of deformed droplets have been studied. The steep gradient

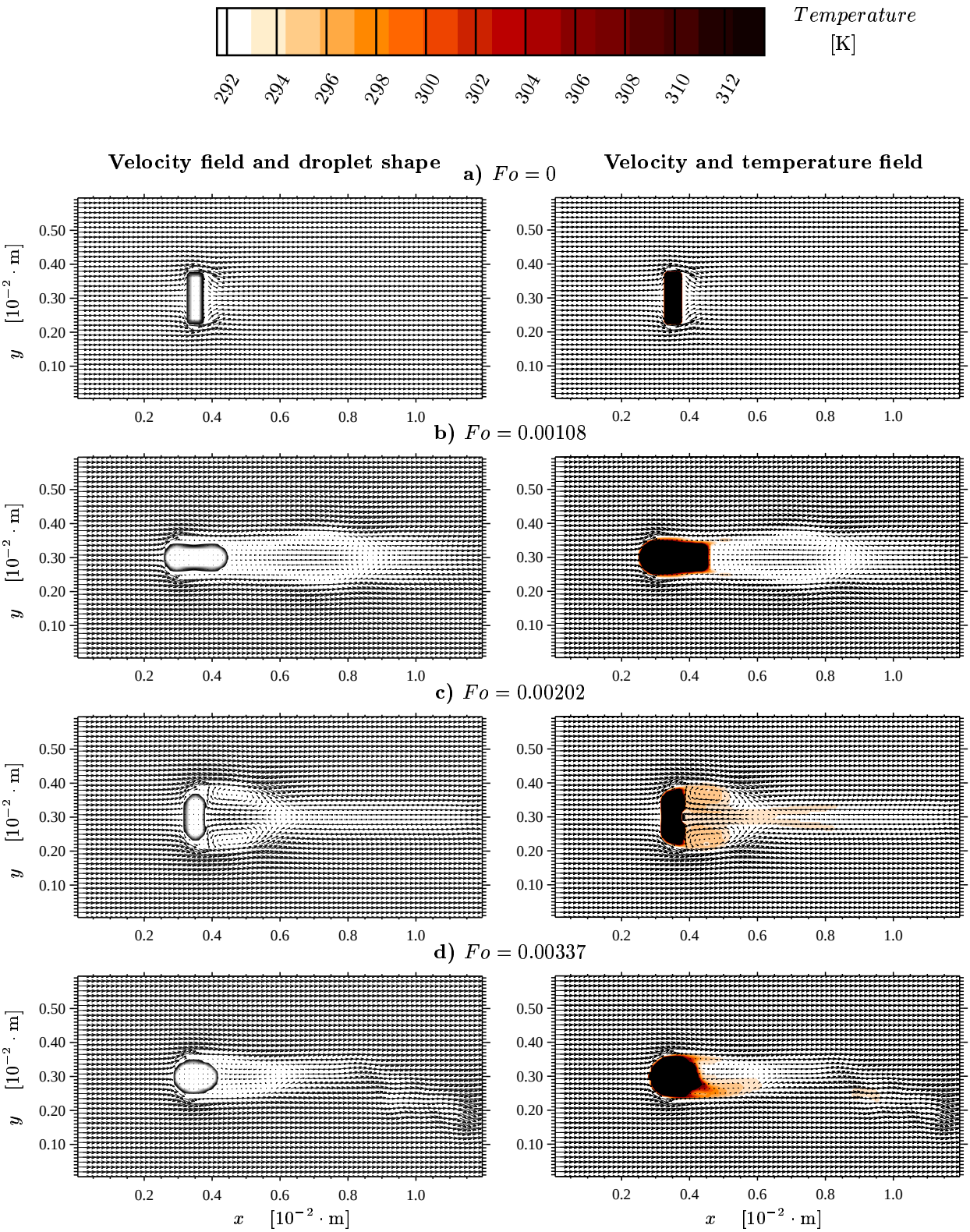

FIGURE 4: Velocity field and temperature field around an initial discoidal droplet with the diameter $D = 1 \cdot 10^{-3}$ in dependency of Fo.

at the beginning of the mean Nusselt number Nu_m evolution in Fig. 5 occurs due to the initial temperature conditions which lead to an infinite temperature gradient and a resulting infinite Nusselt number. In the further evolution of Nu_m. The influence of the deformation can be seen from the peaks in the curves of the initial deformed droplets. The displayed peaks only occur due to the enhanced heat transfer by the motion of the droplets, because the larger surface area of the deformed droplets has taken into in the computation of the Nusselt number (see the calculation of the heat flux density, Eq. (8)). A comparison between the Nusselt

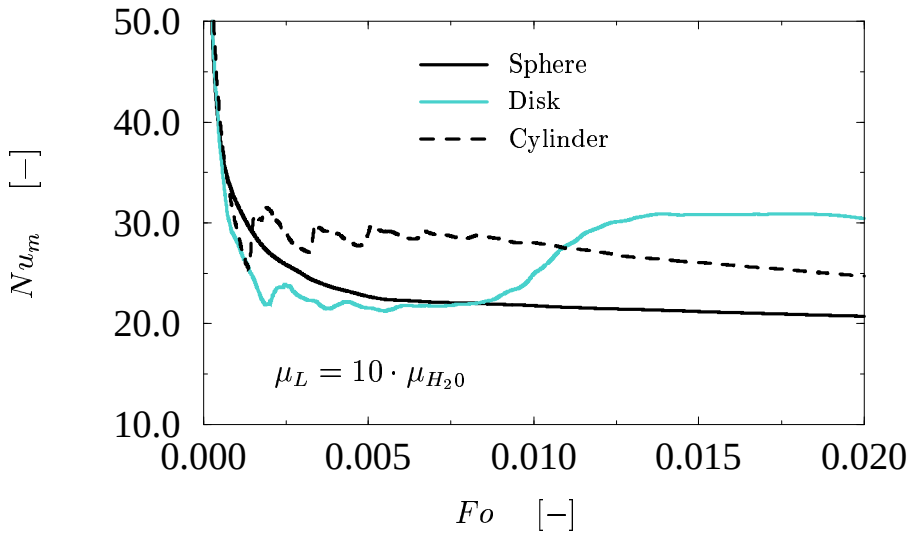

FIGURE 5: Comparison of time and space averaged Nusselt numbers Nu_m for three initial droplet shapes in dependency of Fo.

number computed with the real surface area and with the surface area of a spherical droplet, is given in [7]. The increase of the Nusselt number for the initial discoidal case at $Fo > 0.09$ can be attributed to the history of the discoidal droplet. At this time the interior droplet fluid with a higher temperature is transported to the droplet surface and the resulting higher temperature gradients lead to a higher Nusselt number. To verify this behavior more investigations about the fluid motion in the droplet will be performed.

In Fig. 6 the time dependent, spatial averaged Nusselt number Nu_t for a initial cylindrical droplet is displayed in dependency of Fo. As a reference Nu_t for a spherical droplet is also shown in Fig. 6. A comparison with the plot of the surface area of the cylindrical droplet in Fig. 2 shows that the largest peaks occur in the time period between the spherical to the oblate shape. During this process, the hydrodynamic and the thermal boundary layer are very thin due to the axial velocity of the droplet motion. The thin boundary layers lead to steep gradients in the temperature at the droplet surface and therefore, to higher heat transfer rates. The same behavior can be seen for the discoidal droplet, which is described in [8].

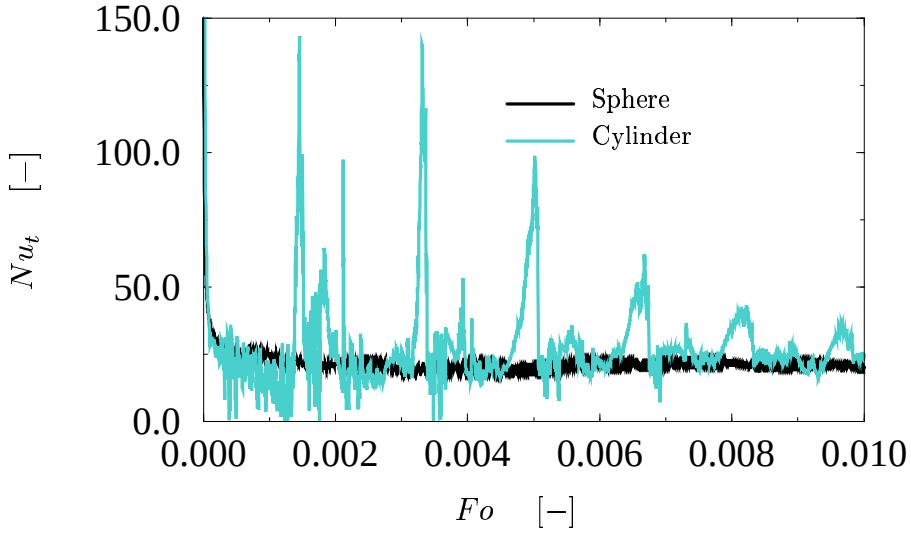

FIGURE 6: Time dependent Nusselt numbers of an initial cylindrical and spherical droplet with $\mu_L = 10 \cdot \mu_{H_2O}$ in dependency of Fo .

Concluding Remarks

A 3D CFD program has been used to compute the heat transfer on initial deformed droplets at high Reynolds number. For the first short period a significant higher heat transfer of the cylindrical droplet in

comparison to the discoidal droplet has been found. A comparison of the temperature fields around a droplet with a time dependent Nusselt number showed that the highest heat transfer occurs during the oscillation from spherical to oblate shape. The results for the time and spatial averaged Nusselt number of a disk showed an increase in Nu_m which is attributed to the change in the internal flow and temperature field. Therefore a detailed investigation of the internal flow field will be performed in the near future in order to analyze these effects in more detail.

Acknowledgments

The authors would like to thank the "Deutsche Forschungsgemeinschaft" (DFG) for the financial support of this project and the High-Performance-Computing-Centre Stuttgart (HLRS) for the computational time on the Cray T3E.

References

[1] M. Rieber and A. Frohn. A numerical study on the mechanism of splashing. *International Journal of Heat and Fluid Flow*, pp. 1–7, 1999.

[2] M. Hase and B. Weigand. Numerical study of the temperature field of unsteady moving droplets and of the surrounding gas. In *Proceedings ILASS-Europe 2001*, Zuerich, 2001.

[3] C.W. Hirt and B.D. Nichols. Volume of fluid (VOF) method for the dynamics of free boundaries. *Journal of computational physics*, Vol. 39, pp. 201–225, 1981.

[4] W.J. Rider and D.B. Kothe. Reconstructing volume tracking. *Journal of computational physics*, Vol. 141, pp. 112–152, 1998.

[5] M. Rieber, F. Graf, M. Hase, N. Roth, and B. Weigand. Numerical simulation of moving spherical and strongly deformed droplets. In *Proceedings ILASS-Europe 2000*, 2000.

[6] R. Scardovelli and S. Zaleski. Direct numerical simulation of free-surface and interfacial flow. *Annual Review Fluid Mechanics*, Vol. 31, pp. 567–603, 1999.

[7] M. Hase and B. Weigand. Direct numerical simulation of flow and heat transfer of a droplet with transient deformation due to the surrounding gas stream. In *Proceedings WCCM V.*, Wien, 2002. http://wccm.tuwien.ac.at/.

[8] M. Hase. Numerische Berechnung dreidimensionaler Transportvorgänge an angeströmten, sich verformenden Tropfen, kleinen Tropfengruppen und Flüssigkeitsligamenten. Technical Report We-2549/1-1, DFG, 2001.